SI Appendix

1. Supporting Materials and Methods

1.1 Samples

Mononucleosomes were reconstituted on a 170-bp-long DNA fragment containing the SELEX 601 positioning sequence (1) and unmodified recombinant *X. laevis* histones. The details of the preparation can be found in ref. 2. DNA fragments were prepared by PCR using primers labeled with Alexa488 and Alexa594 (Purimex, Grebenstein, Germany) and the PCR Master Kit from Promega (Madison, WI). The template pgem3z601 was kindly provided by Jon Widom from Northwestern University. The primers were:
5'-catgcacaggatgtatatatctgacacgtgcct(Alexa594)ggagac-3' and
5'-accctatacgcggccgccctggagaatcccggtgccgaggccgct(Alexa488)caattg-3'.
Both fluorophores were attached via aminolink-C6 linkers. In the intact nucleosome both fluorophores are located on opposite turns of the two superhelical DNA gyres (see Fig. 1*B*). The complete sequence can be found in our previous work (3). After PCR DNA was purified by isopropyl alcohol precipitation and gel filtration with NAP-5 columns (Pharmacia), concentrated to 0.1-0.5 mg/ml in TE (10 mM Tris, 0.1 mM EDTA, pH 7.5) in a vacuum centrifuge and checked on an 8% polyacrylamide gel and with absorption spectroscopy. Preparation of recombinant *X. laevis* histone octamers followed the procedure described in refs. 4 and 5. Nucleosomes were reconstituted by mixing labeled DNA and histone octamer at a molar ratio of 1:1.4 in TE, pH 7.5, and 2 M NaCl. Salt step dialysis was carried out at 4°C with steps of 1.8 M, 1.4 M, 1 M, 0.8 M, 0.6 M, 0.4 M, 0.2 M, 0.1 M for 50 min each. Nucleosomes were finally dialyzed against 5 mM NaCl overnight. Reconstitution efficiency were checked by quantitative agarose gel electrophoresis to measure bound to free DNA ratio and yielded typically >80% intact nucleosomes. Nucleosome positioning properties were checked on a native polyacrylamide gel and with restriction analysis as described in ref. 3. Nucleosome titration experiments were performed on a single-molecule set-up described in ref. 2. 50 pM labeled nucleosomes were diluted in TE buffer (10 mM Tris, 0.1 mM EDTA, pH 7.5) supplemented with 100 mM NaCl, 1 mM ascorbic acid, 0.1 g/L BSA, and an excess of unlabeled nucleosomes. Samples were carefully mixed and data were taken for 1 hour.

1.2 Measurement conditions of single-molecule multiparameter fluorescence detection

The experiments were carried out with a confocal epi-illuminated set-up (FCS-diffusion time of free dye rhodamine 110 t_{Diff} = 0.21 ms) (6, 7). The fluorescently labeled complexes were

excited by a linearly polarized, active-mode-locked argon-ion laser (476 nm, 73 MHz, 150 ps). The laser was focused into the dilute solution (<50 pM) of labeled nucleosome complexes by a 60× water immersion objective. Each molecule generates a brief burst of fluorescence photons as it traverses the detection volume. This photon-train is divided initially into its parallel and perpendicular components via a polarizing beamsplitter and then into wavelength ranges below and above 595 nm. Additionally, red (HQ 630/60 nm) and green (HQ 520/66 nm) filters are in front of the detectors to ensure that only fluorescence photons coming from the acceptor (Alexa594) and donor (Alexa488) dyes are registered. Correction factors l_1 = 0.0308 and l_2 = 0.0368 are used to account for the mixing of polarization by the microscope objective and G factors (G_{Green} = 0.989 for the green channels and G_{Red} = 1.120 for the red channels) are applied to compensate for the slightly different detection efficiency of the two polarization components. Detection is performed using four avalanche photodiodes (SPCM-AQR-14, Laser Components, Germany, for the red channels, and PDM050CTC, MPD, Italy, for the green channels). The signals from all detectors are passed through a passive delay unit and two routers to two synchronized time-correlated single-photon counting boards (SPC 132, Becker and Hickl, Germany) which are connected to a PC. Fluorescence bursts are distinguished from the background of 3-3.5 kHz by applying certain threshold intensity criteria (0.1-ms interphoton time, 150 photons minimum per burst) (6).

2. Supporting Theory for FRET Analysis

2.1 Calculation for FRET parameters

FRET occurs between two fluorophores when the emission spectrum of an excited donor (D) fluorophore overlaps with the absorption spectrum of a nearby acceptor (A) fluorophore. The efficiency, E, of FRET depends strongly on the interdye distance R_{DA} and the Förster radius, R_0 (Eq. 1).

$$E = \left[1 + \left(\frac{R_{DA}}{R_0}\right)^{1/6}\right]^{-1} \qquad \textbf{[1]}$$

Each fluorophore pair has a characteristic Förster radius, R_0, which accounts for the system properties. For the Alexa488-Alexa594 pair in water we estimated R_0 = 55.6 Å.

The efficiency of energy transfer is related to fluorescence lifetimes through (8)

$$E = 1 - \frac{\tau_{D(A)}}{\tau_{D(0)}} \qquad \textbf{[2]}$$

Energy transfer efficiency is experimentally calculated from the fluorescence intensity of the donor, F_D, and acceptor, F_A, (Eq. **3**)

$$E = \frac{F_A \Phi_{FD(0)}}{F_D \Phi_{FA} + F_A \Phi_{FD(0)}} \quad \textbf{[3]}$$

where $\Phi_{FD(0)}$ is the donor fluorescence quantum yield without acceptor and Φ_{FA} is the acceptor fluorescence quantum yield.

To obtain fluorescence intensity of donor and acceptor, the signal intensities (S_G and S_R) were corrected for mean background counts (typically between 2 and 2.3 kHz for the green channels, $\langle B_G \rangle$ (donor), and 1and 1.2 kHz for the red channels, $\langle B_R \rangle$ (acceptor)), spectral crosstalk, α (0.07), direct excitation of the acceptor, DE (1.35kHz) and the ratio of the detection efficiencies, g, between the green and red channels (g_G/g_R = 0.58) (Eq. **4**).

$$F_D = \frac{S_G - \langle B_G \rangle}{g_G} = \frac{F_G}{g_G}$$

$$F_A = \frac{S_R - (\langle B_R \rangle + DE) - \alpha(S_G - \langle B_G \rangle)}{g_R} = \frac{F_R}{g_R} \quad \textbf{[4]}$$

Fluorescence lifetime is determined for each burst using a maximum likelihood estimator (MLE) and iterative convolutions to account for the scatter contribution (6). The lifetime of the donor dye ($\tau_{D(0)}$) coupled to the nucleosomal DNA in absence of the acceptor was determined to be 4.1 ns.

2.1.1. Calculation of expected FRET efficiency by using MD simulations

Molecular dynamics (MD) simulations provide "clouds" of possible positions of the dyes (9); see also *Section 2.6*. From these data it is possible to calculate the mean position FRET efficiency, E_{mp}, as:

$$E_{mp} = \frac{R_0^6}{R_0^6 + R_{mp}^6} \quad \textbf{[5]}$$

However, due to the flexibility of the fluorophore linker R_{mp} is not directly accessible in FRET experiments. What is measured in the experiment is the isotropic average FRET efficiency (9), $\langle E \rangle_{iso}$, that is the average over all FRET efficiencies calculated from all the possible donor-acceptor distances R_i. $\langle E \rangle_{iso}$ is calculated as:

$$\langle E \rangle_{iso} = \left\langle \frac{R_0^6}{R_0^6 + R_i^6} \right\rangle \quad \textbf{[6]}$$

2.2 Dye linker flexibility

In the case of a dynamic system, in which a molecule during the transit in the focus can switch between different states, each characterized by a transfer efficiency *E*, the lifetime calculated by MLE (10) is a fluorescence intensity weighted average lifetime:

$$\tau_{ave,a} = \sum_i a_i \tau_i \qquad \text{with} \qquad a_i = \frac{x_i \tau_i}{\sum_i x_i \tau_i} \qquad \textbf{[7]}$$

In Eq. **7**, τ_i is the fluorescence lifetime of the *i*th state and x_i is the fraction of time the molecule spends in the *i*th state. On the other hand, *E* is a species-weighted average:

$$E_{ave,x} = \sum_i x_i E_i \qquad \textbf{[8]}$$

For this reason, in the presence of dynamic processes Eq. **2** does not hold anymore and a correction must be performed. In our nucleosome measurements we observed a deviation from the behavior of Eq. **2** that could be easily explained with a fast dynamic fluctuation of distances. We interpreted this fluctuation as the effect of dye linker flexibility. To test this hypothesis we first considered that each mean distance R_{DA} appears in reality as two distances $R_{DA} \pm \sigma$, where σ (= 6 Å) is the displacement due to the linker flexibility. The value of σ = 6 Å is consistent with the results of bulk TCSPC measurements on shorter DNA fragments (unpublished results). Then we calculated the fluorescence-weighted average and the species-weighted average, $\tau_{ave,x} = \sum_i x_i \tau_i$ (that would satisfy Eq. **2**). By polynomial fitting of $\tau_{ave,x}$ plotted as a function of $\tau_{ave,a}$ we obtained an equation that would *convert* one average into the other (Eq. **9**)

$$\tau_{ave,x} = 0.00479 + 0.4813\tau_{ave,a} + 0.26694\tau_{ave,a}^2 - 0.03435\tau_{ave,a}^3 \qquad \textbf{[9]}$$

and substituted it into Eq. **2**

$$E = 1 - \frac{0.00479 + 0.4813\tau_{ave,a} + 0.26694\tau_{ave,a}^2 - 0.03435\tau_{ave,a}^3}{\tau_{D(0)}} \qquad \textbf{[10]}$$

2.3 Probability distribution analysis (PDA)

As shown by Antonik et al. (11), PDA can be simplified if each fluorescence burst is first divided into bins of equal length, i.e., time windows. To handle multimolecular events properly (12), we analyzed the entire photon stream without applying any burst selection beforehand. In addition, each data set was studied by globally fitting time windows of two different lengths, 1 ms and 3 ms.

The time windows in Fig. S2 *C* and *D* are fitted equally well using the same set of parameters; therefore we can exclude the presence of dynamical processes with timescale comparable to the dwell time of the nucleosome in the focus.

Histograms of donor-acceptor distances, R_{DA}, and FRET efficiencies, E, were calculated from experimental data sets according to Eqs. **3** and **11** (13)

$$R_{DA} = R_0 \left(\frac{\Phi_{FA} F_D}{\Phi_{FD(0)} F_A} \right)^{1/6} \qquad \textbf{[11]}$$

Fits to experimental histograms were generated by applying Eqs. **3**, **4**, and **11** to theoretical distributions $P(S_G, S_R)$ which were calculated by using the reported PDA theory (11, 14). The experimental histograms were fitted using a four-state model to account for donor-only species and the three FRET species (*LF*, *MF*, and *HF*). A single-distance model was not sufficient to describe the FRET states; this could be due to numerous experimental artefacts (11, 15) and/or complex acceptor dye photophysics. Thus, each FRET state was fitted using an (apparent) Gaussian distribution of distances, with a mean of R_{DA} (center of the Gaussian distribution) and a half-width, HW.

2.3.1 Correction of PDA model functions for the presence of direct excitation

Let us assume that the direct excitation probability is p_{DE} as shown in Scheme 1

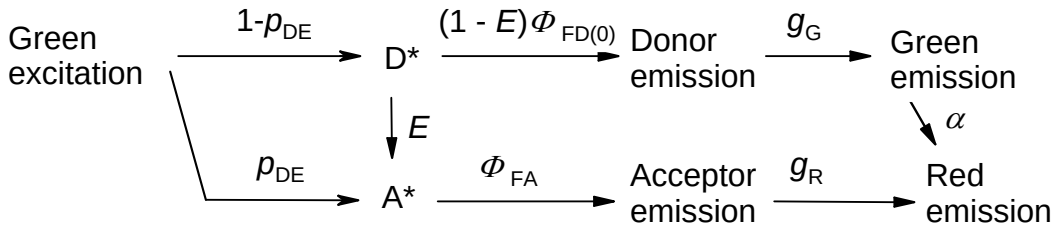

Scheme 1. Excitation and emission pathways entering the PDA model function, Eq. **12**.

Scheme 1 shows all processes considered in PDA together with their probabilities. It follows directly from Scheme 1 that a probability of a detected photon being green is

$$\begin{aligned} p_G &= \frac{(1-p_{DE})(1-E)\Phi_{FD(0)} g_G}{(1+\alpha)(1-p_{DE})(1-E)\Phi_{FD(0)} g_G + (p_{DE} + (1-p_{DE})E)\Phi_{FA} g_R} \\ &= \left(1 + \alpha + \frac{(p_{DE}(1-p_{DE})^{-1} + E)\Phi_{FA}}{(1-E) G \Phi_{FD(0)}} \right)^{-1} \end{aligned} \qquad \textbf{[12]}$$

Eq. **12** replaces Eq. 3 in ref. 12.

2.4 Confidence intervals estimation in PDA

2.4.1 Chi-squared surfaces

χ_r^2 surfaces, Fig. S2*E*, represents 2D plots of the reduced chi-squared values χ_r^2 against any two fit parameters while keeping other parameters fixed at their optimal values (16). Assuming no or little correlation between the two plotted and remaining fit parameters (which might not be the case, see next subsection), χ_r^2 surfaces allow for estimation of error intervals (16).

2.4.2 Error limits for multiple parameters

Alternatively, we varied all free fit parameters of the fit in a random manner. The χ_r^2-value was calculated at 10,000 to 50,000 random points, yielding 20-1,000 points with χ_r^2 values within $\pm(2/N_{bins})^{1/2}$ of that of the optimal fit (17). Parameter intervals where such fits were possible were assigned as confidence intervals, as presented in Table S1 for the case of 25 mM NaCl. Other data sets discussed in the main text were of comparable data quality and there was therefore no reason to expect significantly different error limits. In most of cases the presented error limits are consistent with those obtained from χ_r^2 surfaces.

2.4.3 Systematic errors due to crosstalk and direct excitation

The spectral crosstalk and the direct excitation (Eq. **12** and Scheme 1) significantly contribute to the red signal. To investigate the influence of these parameters on fit results, we fixed the values of crosstalk and direct excitation probability at "wrong" values and fitted the data as usually. We found that that a 10% relative systematic error in crosstalk and direct excitation would result in approximately 6-Å and 4-Å errors in the longer distance R_{DA} (i.e., that of *LF* species), respectively.

2.4.4 Distances beyond the FRET range

In some cases, PDA fits produce mean distances well beyond the maximum distance measurable by FRET. Intuitively this seems to be conflicting with the well-known conception of the distance range accessible to FRET being roughly within $0.5R_0$ to $2R_0$ (18). To explain this fact one should note that the modeled distance distributions are so broad that the mean FRET efficiency is actually measurable. For instance, for R_{DA} = 120 Å and half-width HW = 30 Å small changes in either R_{DA} or HW can change $\langle E \rangle$ by 1-2%, which is easily detected by PDA (11).

Considering a Gaussian distribution of distances $P(r_{DA})$ with a mean (center) distance R_{DA} and a half-width HW, the mean FRET efficiencies $\langle E \rangle$ were calculated according to Eq. **13**

$$\langle E \rangle = \int_0^{+\infty} P(r_{DA}) E(r_{DA}) dr_{DA} = \int_0^{+\infty} \frac{1}{\mathrm{HW}\sqrt{2\pi}} \exp\left(\frac{-(r_{DA} - R_{DA})^2}{2(\mathrm{HW})^2} \right) \frac{1}{1 + (r_{DA} / R_0)^6} dr_{DA} \quad \textbf{[13]}$$

2.5 Species-selective filtered fluorescence correlation spectroscopy (fFCS)

Fluorescence correlation spectroscopy, FCS, is a powerful method to determine the diffusion time of a fluorescently labeled molecule and study all those processes that lead to a fluctuation in the fluorescence signal. The obtained correlation curves were fitted with a model taking into account translational diffusion, triplet formation, and an additional correlation term, bunching term, whose nature we did not investigate in this work:

$$G(t_C) = 1 + \frac{1}{N} \cdot \left(1 + \frac{t_C}{t_{Diff}} \right)^{-1} \cdot \left(1 + \left(\frac{\omega_0}{z_0} \right)^2 \cdot \frac{t_C}{t_{Diff}} \right)^{-\frac{1}{2}} \cdot \left(1 + \frac{T}{(1-T)} \cdot \exp(-t_C / t_T) \right) \cdot \left(1 + \frac{B}{(1-B)} \cdot \exp(-t_C / t_B) \right)$$

[14]

where N is the average number of molecules in the detection volume, t_{Diff} is the diffusion time, z_0 and ω_0 are the $1/e^2$ radii in the axial and radial direction respectively, T is the amplitude of the triplet, t_T is the characteristic time of the triplet, B is the amplitude (fraction) of the second bunching term, and t_B is the characteristic time of that bunching term. Knowing the shape and size of the focal volume, it is possible to calculate the diffusion coefficient, D, as:

$$D = \frac{\omega_0^2}{4 \cdot t_{Diff}} \quad \textbf{[15]}$$

By fitting Eq. **14** it is possible to know the average number of molecules present in the focal volume; however, in the case FCS performed at single-molecule concentration, the presence of scatter photons influences the amplitude of the correlation curve, leading to an incorrect evaluation of N (6). When more than one FRET species are simultaneously present in solution, Eq. **14** does not hold anymore. For a mixture of species, in fact, the correlation function becomes

$$G(t_C) = 1 + \frac{1}{N} \cdot \frac{\sum_i^n x_i \cdot Q_i^2 \cdot G_i^2(t_C)}{\left(\sum_i^n x_i \cdot Q_i \right)^2} \quad \textbf{[16]}$$

where x_i is the fraction of the ith species, Q_i is its brightness, and $G_i^2(t_C)$ its normalized correlation function. In this case, even knowing exactly the brightness of each species, it will be very difficult to sort them correctly if their diffusion times do not differ significantly.
To solve this problem Enderlein and co-workers (19-21) have suggested using the fluorescence lifetime decay pattern of the different species to build filters that will attribute to each photon a certain likelihood, even negative, that said photon belongs to a determined species. By applying the filters only those photons that belong to the same species will be correlated; and by using the instrumental response function as an additional pattern it is possible to eliminate the contribution of scattered photons and compute the correct correlation amplitudes even at single-molecule concentrations.

2.5.1 Building the filters

For simplicity, we consider the mixture of two molecular species measured with a confocal microscope set-up as the one used for this work (as described in *Section 1.2*). The fluorescence filters for filtered FCS are generated as described in ref. 22.
The fluorescence lifetime filters can be devised not only for two different polarizations of the same spectral range, but also for any combination of polarization and spectral range. For this work the filters were built using the lifetime pattern of both green and red channels, and the correlation was computed only for the parallel polarisation, $G^{(i)}_{(G_\parallel+R_\parallel)(G_\parallel+R_\parallel)}(t_c)$.

2.5.2 Selecting the species

To obtain the decay pattern of the different species we performed subensemble analysis (23) by selecting the fluorescence bursts in the $\tau_{D(A)}$ versus S_G/S_R 2D plot as the ones in Fig. 2 *A* and *B* of the main text. Due to the close similarity between the decay patterns, Donor-only and *LF* are grouped together, and the *HF* and *MF* species are grouped in the FRET species. The instrument response function was used as additional species to get rid of scatter photons.

2.6 Modeling

2.6.1 Modeling the fluorophore position cloud obtained from MD simulations to the nucleosomal DNA structure

To compare the nucleosome structure with our data, we modeled the fluorophore position clouds obtained from the MD simulation of a straight B-DNA (9) to the respective bases in the nucleosomal DNA. On a local view, the backbone of the nucleosomal DNA shows

significant deviation from that of the straight DNA. Thus we aligned the positional clouds together with the straight DNA to the nucleosomal DNA by superposing the thymine where the fluorophores are bound. After alignment, all donor position within 2 Å of the histones and all acceptor positions within 4 Å of the histone core were discarded. This procedure left 93% of the original donor cloud and 61% of the original acceptor cloud. The impact on the average orientation of the dye was minimal, and a $\kappa^2 = 0.65$ was calculated.

2.7 Geometric model description of nucleosomes

2.7.1 Continuous model

We assume that both ends of DNA can partly dissociate from the core as shown in Fig. 5. The number of dissociated bases from donor and acceptor sides (N_D and N_A, respectively) can be arbitrary provided at least one base pair remains bound. Internal detachment is not considered. There can be an additional constant separation between the DNA loops along the z-axis, Δz (Fig. 5).Unlike the "discrete" model (see next section and main text), the continuous model does not produce any MF peak (Fig. S3), which is clearly inconsistent with our experimental data.

2.7.2 Discrete (contact point) models

The discrete model accounts for the fact that DNA dissociates stepwise at defined "contact points" (see Fig. 5). The bases that form contact points are selected according to their proximity to the core. From the X-ray structure 12 contact points have been identified within a 4 Å shell from the core, as summarized in Table S3. DNA is therefore assumed to dissociate in steps of 10-11 bp (cf. Table 3). For the model with a step size of 5 bp, we used the contact points identified from the X-ray structure and added an intermediate step.

2.7.3 Model parameters

We need also to calculate x, y, and z components of the DA-distance vector and the effective radius R, which is the distance from the center of the core to the dye cloud's center of mass (Fig. 1*B*). From the X-ray structure we estimate the effective radius of about 39-44 Å (40 Å is assumed in the simulation) and Δz of about 45 Å. Assuming another radius $R = 45$ Å does not significantly change the FRET efficiency pattern shown in Fig. 5 in the main text. In addition, the shifts between the center of mass of the dye clouds and their respective attachment points are taken into account. (approximately 1.5 bp). Other model parameters are effective radius, $R = 40$ Å, 80 bp per turn, DNA length 170 bp, D dye position at 46.5 bp (relative to the donor

strand), A dye position at 136.5 bp (relative to the donor strand), Δz (per turn) = 45 Å. A scaling factor $\beta = 1.1$ for the Förster radius $R_0 = 55.6$ Å is also used in the geometric model to normalize the experimental FRET efficiency of the compact nucleosome to the theoretical one.

Fig. S3 shows that the shape of the *E* distributions becomes increasingly narrow if the step size increases. Only the discrete models are able to reproduce the characteristic FRET peaks of the HF and MF species (see Fig. S3 *E* and *H*). The contrast between HF and MF decreases if smaller steps are allowed.

3. Supporting Results

3.1 PDA fit

The results of the PDA fits for nucleosomes at different salt concentrations (see main text *Section 2.2*) are reported in Table S2a.

From the values tabled in Table S2a it was possible to calculate (Eq. **13**) for each species the average R_{DA} (average $R_{HF} = 54.2$ Å and average $R_{MF} = 63.5$ Å) and the mean FRET efficiency (Table S2b).

3.2 Free DNA and worm-like chain model

In free DNA, the dyes are separated by 93 bp, that is, approximately 300 Å. DNA is not fully rigid; a quantitative dependence of DNA looping probability on the DNA length has been given in ref. 24, where also the effect of this flexibility on transcriptional activation has been discussed. Later, a more thorough analysis gave an expression for the end-to-end distance distribution in DNA (25, 26). We applied this expression to estimate the DA distance distribution $P(r_{DA})$ and concomitantly the mean FRET efficiency expected for the free DNA. In combination with Eq. **13** we used Eq. 2 from ref. 25, which reads

$$P(r_{DA}) = a\, r_{DA} \frac{\exp(-R_s / 8L_p\left[1-(r_{DA}/R_s)^2\right])}{\left[1-(r_{DA}/R_s)^2\right]\left[2-(r_{DA}/R_s)^2\right]^2} \qquad \textbf{[17]}$$

where R_s is the length of fully stretched DNA segment, L_p stands for the DNA persistence length, and a is a normalization factor. Assuming the persistence length of DNA of 530 Å, one obtains $\langle E \rangle \cong 0.01$, which is significantly lower than the measured $\langle E \rangle$ of 0.047 (Table S2b).

3.3 Time evolution of FRET species

To study the evolution of the species with time, the measurement time of each salt condition was divided in time segments (200-300 s), and each segment was fit with PDA by using the four-state model described in the main text. At first, the whole joint data set was analyzed to determine the properties of the individual species (Table S2a). To obtain the individual species fractions $x_{\mathrm{HF}}, x_{\mathrm{MF}}, x_{\mathrm{LF}}, x_{\mathrm{DOnly}}$ in the small time segments, we fixed the structural parameters and varied only the individual fractions. The obtained fractions are shown in Fig. 3*A*.

To characterize the characteristic times of the evolution of *LF*, *HF*, and *MF* species, the fractions obtained from the PDA fit of each NaCl concentration were fitted separately with a global system of equations:

$$\begin{cases} x_{DOnly} = const. \\ x_{HF}(t) = x_{HF}(0) + x_{HF}(\infty)\exp\left[-\dfrac{t}{\tau_{HF}}\right] \\ x_{MF}(t) = x_{MF}(0) + x_{MF}(\infty)\exp\left[-\dfrac{t}{\tau_{MF}}\right] \\ x_{LF}(t) = \left(1 - x_{HF}(0) - x_{MF}(0) - x_{DOnly}\right) + \\ \qquad x_{HF}(\infty)\left(1 - \exp\left[-\dfrac{t}{\tau_{HF}}\right]\right) + x_{MF}(\infty)\left(1 - \exp\left[-\dfrac{t}{\tau_{MF}}\right]\right) \end{cases} \qquad \textbf{[18]}$$

where τ_{HF} and τ_{MF} are the characteristic times of *HF* and *MF* fraction decay, respectively. The results of the fits are reported in Table S4 a and b.

3.4 FCS salt dependence

Nucleosome samples and free DNA samples were measured on different days, with the exception of free DNA at 5 mM NaCl that was measured on both sessions. Because characteristic diffusion times scale with the detection volume (see Eq. **15**) due to the slightly different set-up alignment the characteristic diffusion times cannot be directly compared. To overcome this problem we scaled the results of free DNA so that the diffusion times at 5 mM NaCl from the different days would coincide. The FCS curves of the nucleosome samples, all measured on the same day, are shown in Fig. S4. Each dataset was then divided into two parts and fitted separately. For some salt conditions more than one measurement was available.

From the fit results, average diffusion times and standard deviations were calculated. The reported errors for *LF+DOnly*, *HF+MF*, and free DNA are the averages of the standard deviations obtained for that species at the different NaCl concentrations.

1. Thastrom A, et al. (1999) Sequence motifs and free energies of selected natural and non-natural nucleosome positioning DNA sequences. *J Mol Biol* 288:213-229.
2. Gansen A, Tóth K, Schwarz N, Langowski J (2009) Structural variability of nucleosomes detected by single-pair Förster resonance energy transfer: Histone acetylation, sequence variation, and salt effects. *J Phys Chem B* 113:2604-2613.
3. Gansen A, Hauger F, Tóth K, Langowski J (2007) Single-pair fluorescence resonance energy transfer of nucleosomes in free diffusion: optimizing stability and resolution of subpopulations. *Anal Biochem* 368:193-204.
4. Luger K, Rechsteiner TJ, Richmond TJ (1999) Preparation of nucleosome core particle from recombinant histones. *Methods Enzymol* 304:3-19.
5. Tóth K, Brun N, Langowski J (2006) Chromatin compaction at the mononucleosome level. *Biochemistry* 45:1591-1598.
6. Eggeling C, et al. (2001) Data registration and selective single-molecule analysis using multi-parameter fluorescence detection. *J Biotechnol* 86:163-180.
7. Widengren J, et al. (2006) Single-molecule detection and identification of multiple species by multiparameter fluorescence detection. *Anal Chem* 78:2039-2050.
8. van der Meer BW, Cooker G, Chen SY (1994) *Resonance Energy Transfer: Theory and Data* (VCH, New York).
9. Woźniak AK, Schröder G, Grubmüller H, Seidel CAM, Oesterhelt F (2008) Single molecule FRET measures bends and kinks in DNA. *Proc Natl Acad Sci USA* 105:18337-18342.
10. Maus M, et al. (2001) An experimental comparison of the maximum likelihood estimation and nonlinear least-squares fluorescence lifetime analysis of single molecules. *Anal Chem* 73:2078-2086.
11. Antonik M, Felekyan S, Gaiduk A, Seidel CAM (2006) Separating structural heterogeneities from stochastic variations in fluorescence resonance energy transfer distributions via photon distribution analysis. *J Phys Chem B* 110:6970-6978.
12. Kalinin S, Felekyan S, Valeri A, Seidel CAM (2008) Characterizing multiple molecular states in single-molecule multiparameter fluorescence detection by probability distribution analysis. *J Phys Chem B* 112:8361-8374.
13. Rothwell PJ, et al. (2003) Multi-parameter single-molecule fluorescence spectroscopy reveals heterogeneity of HIV-1 reverse transcriptase:primer/template complexes. *Proc Natl Acad Sci USA* 100:1655-1660.
14. Kalinin S, Felekyan S, Antonik M, Seidel CAM (2007) Probability distribution analysis of single-molecule fluorescence anisotropy and resonance energy transfer. *J Phys Chem B* 111:10253-10262.
15. Nir E, et al. (2006) Shot-noise limited single-molecule FRET histograms: Comparison between theory and experiments. *J Phys Chem B* 110:22103-22124.
16. Bevington PR (1969) *Data Reduction and Error Analysis for the Physical Sciences* (McGraw-Hill, New York).
17. Soong TT (2004) *Fundamentals of Probability and Statistics for Engineers* (Wiley, West Sussex, England).
18. Valeur B (2002) *Molecular Fluorescence: Principles and Applications* (Wiley-VCH, Weinheim, Germany).

19. Böhmer M, Wahl M, Rahn HJ, Erdmann R, Enderlein J (2002) Time-resolved fluorescence correlation spectroscopy. *Chem Phys Lett* 353:439-445.
20. Enderlein J, Gregor I (2005) Using fluorescence lifetime for discriminating detector after pulsing in fluorescence-correlation spectroscopy. *Rev Sci Instrum* 76:033102.
21. Kapusta P, Wahl M, Benda A, Hof M, Enderlein J (2007) Fluorescence lifetime correlation spectroscopy. *J Fluoresc* 17:43-48.
22. Felekyan S, Kalinin S, Valeri A, Seidel CAM (2009) Filtered FCS and species cross correlation function. *Proc SPIE* 7183:71830D.
23. Neubauer H, et al. (2007) Orientational and dynamical heterogeneity of rhodamine 6G terminally attached to a DNA helix revealed by NMR and single-molecule fluorescence spectroscopy. *J Am Chem Soc* 129:12746-12755.
24. Rippe K, von Hippel PH, Langowski J (1995) Action at a distance: DNA-looping and initiation of transcription. *Trends Biochem Sci* 20:500-506.
25. Valle F, Favre M, De Los Rios P, Rosa A, Dietler G (2005) Scaling exponents and probability distributions of DNA end-to-end distance. *Phys Rev Lett* 95:158105.
26. Winkler RG (2003) Deformation of semiflexible chains. *J Chem Phys* 118:2919-2928.